IEEE Access
Multidisciplinary | Rapid Review | Open Access Journal

Received December 7, 2019, accepted December 26, 2019, date of publication January 6, 2020, date of current version January 14, 2020.

Digital Object Identifier 10.1109/ACCESS.2020.2964385

Modeling Floating Potential Conductors Using Discontinuous Galerkin Method

LIANG CHEN, (Member, IEEE), MING DONG, (Student Member, IEEE), AND HAKAN BAGCI, (Senior Member, IEEE)

Division of Computer, Electrical, and Mathematical Science and Engineering, King Abdullah University of Science and Technology (KAUST), Thuwal 23955-6900, Saudi Arabia

Corresponding author: Liang Chen (liang.chen@kaust.edu.sa)

This work was supported by the King Abdullah University of Science and Technology (KAUST) Office of Sponsored Research (OSR) under Award 2016-CRG5-2953.

ABSTRACT Isolated conductors appear in various electrostatic problems. In simulations, an equipotential condition with an undefined/floating potential value is enforced on the surface of isolated conductors. In this work, a numerical scheme making use of the discontinuous Galerkin (DG) method is proposed to model such conductors in electrostatic problems. A floating-potential boundary condition, which involves the equipotential condition together with a total charge condition, is ''weakly'' enforced on the conductor surfaces through the numerical flux of the DG method. Compared to adaptations of the finite element method used for modeling conductors, this proposed method is more accurate, capable of imposing charge conditions, and simpler to implement. Numerical results, which demonstrate the accuracy and applicability of the proposed method, are presented.

INDEX TERMS Discontinuous Galerkin method, electrostatics, finite element method, floating potential conductors, magnetostatics, plasmonic-enhanced photoconductive antenna.

I. INTRODUCTION

In electrostatic simulations, a perfect conductor is used to approximate a metallic body with a very high conductivity and its surface is assumed to be equipotential. Furthermore, in many applications these conductors are isolated, in other words, the value of the potential on their surface is not defined or fixed [1]–[10]. For example, electrode core of high-voltage inductors [1], floating electrodes of IEC surge arresters [2], defects in ultra-high-voltage gas-insulated switchgear [3], passive electrodes of earthing systems [4], conductor of floating-gate transistors [5], plasma analyzer for spacecraft floating potential measurements [6], and metallic nanostructures in optoelectronic devices [7] can all be modeled as isolated conductors in electrostatic simulations. In the rest of this paper, these conductors are referred to as floating-potential conductors (FPCs).

Various methods have been developed to incorporate FPC models in electrostatic simulations. For unbounded problems with homogeneous or piece-wise homogeneous materials, the boundary element method (BEM) is often preferred [2], [9]. In [2] a total electric charge condition is applied to determine the potential of uncharged floating electrodes. In [9], the Poincare-Steklov operator is used to enforce constraints corresponding to the floating potential. For more complex systems with inhomogeneous materials, the finite element method (FEM) is widely used [10]–[17].

Several techniques have been introduced to the traditional FEM so that FPCs can be accounted for. These include the virtual permittivity method (VPM) [10], the matrix reduction method (MRM) [13], and the charge simulation method (CSM) [11], [12], [16]. These methods' accuracy, ease of implementation (or amount of modifications required for implementation in legacy FEM codes), ability to account for charges on FPCs, and savings in the number of unknowns have recently been compared in [15]. Among all the schemes used for analyzing problems involving FPCs, VPM is perhaps the easiest one to implement since it does not require any modifications to the traditional FEM code. However, its accuracy depends on the proper selection of the ''virtual'' permittivity. Accurate representation of an FPC requires a very high virtual permittivity value but this in return reduces the solution accuracy since it makes the FEM matrix ill-conditioned. MRM does not suffer from this problem but

The associate editor coordinating the review of this manuscript and approving it for publication was Mengmeng Li.

This work is licensed under a Creative Commons Attribution 4.0 License. For more information, see http://creativecommons.org/licenses/by/4.0/

it requires considerable modifications to the original FEM code [13]–[15]. Additionally, both VPM and MRM lack the ability to enforce nonzero charge conditions on the surface of an FPC [13]–[15]. CSM can account for charge conditions but setting a specific charge distribution on an FPC calls for a priori knowledge often acquired heuristically by running multiple simulations [13]–[16].

In this work, we propose a scheme that permits the discontinuous Galerkin (DG) method [18]–[20] to account for FPCs. This scheme "weakly" enforces both the equipotential condition and the charge condition (on the total electric field intensity) on the surface of an FPC using the numerical flux of DG. In the rest of the paper, the combination of these two conditions is referred to as the floating potential boundary condition (FPBC). The implementation of the FPBC is similar to that of the Dirichlet boundary condition and requires only subtle modifications to the original DG code. In addition, by effectively "replacing" an FPC with its FPBC, the need for an internal mesh discretizing the FPC is eliminated, and the inaccuracy problem that would be introduced by a virtual permittivity is avoided. It should also be noted here that the proposed formulation naturally handles multiple isolated conductors with independent charge conditions. The properties of the proposed method are summarized and compared to those of the other methods in Table. 1.

TABLE 1. Comparision of FEM-based methods used for modeling FPC.

	VPM	MRM	CSM	DG-FPBC
Charge condition	no	no	yes	yes
Accuracy	no	yes	no	yes
Easy implementation	yes	no	no	yes
No interal mesh	no	(yes)	no	yes

The rest of the paper is organized as follows. Section II starts with the formulation of DG for the Poisson equation. This is followed by introduction of the FPBC into DG framework and description of its discretization. In Section III, the proposed method is validated through comparison of the results computed for a canonical problem to those obtained from analytical expressions. Its applicability of the method is further demonstrated through its application to the analysis of a realistic optoelectronic semiconductor device. Section IV provides a summary and discusses possible future research directions.

II. FORMULATION

A. MATHEMATICAL MODEL

Consider the electrostatic problem described in Figure 1. M isolated conductors $\Omega_1^C, \Omega_2^C, \ldots, \Omega_M^C$ are distributed in domain Ω. Surface of each conductor and the charge on it are represented by $\partial\Omega_\eta^C$ and Q_η^C, $\eta = 1, 2, \ldots M$, respectively. Domain Ω is bounded by surface $\partial\Omega$: $\partial\Omega = \partial\Omega^D \cup \partial\Omega^N$, where $\partial\Omega^D$ and $\partial\Omega^N$ represent the boundaries where Dirichlet and Neumann boundary conditions are enforced,

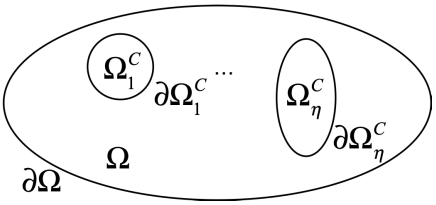

FIGURE 1. Schematic description of an electrostatic problem involving multiple isolated conductors.

respectively. This electrostatic problem is expressed in the form of a boundary value problem (BVP)

$$\nabla \cdot [\varepsilon(\mathbf{r})\nabla\varphi(\mathbf{r})] = -\rho(\mathbf{r}), \quad \mathbf{r} \in \Omega \tag{1}$$

$$\varphi(\mathbf{r}) = f^D(\mathbf{r}), \quad \mathbf{r} \in \partial\Omega^D \tag{2}$$

$$\hat{\mathbf{n}} \cdot \varepsilon(\mathbf{r})\nabla\varphi(\mathbf{r}) = f^N(\mathbf{r}), \quad \mathbf{r} \in \partial\Omega^N, \tag{3}$$

$$\varphi(\mathbf{r}) = \varphi_\eta^C, -\oint_{\partial\Omega_\eta^C} \hat{\mathbf{n}} \cdot \varepsilon(\mathbf{r})\nabla\varphi(\mathbf{r})d\mathbf{r} = Q_\eta^C, \quad \mathbf{r} \in \Omega_\eta^C. \tag{4}$$

In (1)-(4), $\varphi(\mathbf{r})$ is the electric potential distribution to be solved for, $\varepsilon(\mathbf{r})$ is the permittivity, $\rho(\mathbf{r})$ is the charge density, $f^D(\mathbf{r})$ and $f^N(\mathbf{r})$ are the coefficients associated with the Dirichlet and Neumann boundary conditions, respectively, and $\hat{\mathbf{n}}$ denotes the outward normal vector of the corresponding surface. Equation (4) represents the physical conditions on FPCs. We note that on each FPC, the equipotential value φ_η^C is an unknown. Physically, φ_η^C changes with the total charge Q_η^C of the conductor. φ_η^C is uniquely determined by the charge condition in (4), i.e., the total electric flux is equal to the total charge.

B. DISCONTINUOUS GALERKIN FORMULATION

In this subsection, we discuss the DG scheme used for discretizing the BVP described by only (1)-(3). Then we introduce the FPBC (4) with some necessary modifications in the next subsection. To facilitate the numerical solution of the BVP (1)-(3), we use the electric field $\mathbf{E}(\mathbf{r}) = -\nabla\varphi(\mathbf{r})$ to reduce the order of the spatial derivative. Equation (1)-(3) can be rewritten as

$$\nabla \cdot [\varepsilon(\mathbf{r})\mathbf{E}(\mathbf{r})] = \rho(\mathbf{r}), \quad \mathbf{r} \in \Omega \tag{5}$$

$$\mathbf{E}(\mathbf{r}) = -\nabla\varphi(\mathbf{r}), \quad \mathbf{r} \in \Omega \tag{6}$$

$$\varphi(\mathbf{r}) = f^D(\mathbf{r}), \quad \mathbf{r} \in \partial\Omega^D \tag{7}$$

$$-\hat{\mathbf{n}} \cdot \varepsilon(\mathbf{r})\mathbf{E}(\mathbf{r}) = f^N(\mathbf{r}), \quad \mathbf{r} \in \partial\Omega^N. \tag{8}$$

BVP (5)-(8) is solved with the local DG (LDG) method [18], [21], [22]. First, Ω is discretized into K non-overlapping tetrahedrons. The volumetric support of each of these elements is represented by Ω_k, $k = 1, \ldots, K$. Let $\partial\Omega_k$ denote the element surface of Ω_k and $\hat{\mathbf{n}}(\mathbf{r})$ denote the outward unit vector normal to $\partial\Omega_k$. Then, (5)-(6) are tested with Lagrange polynomials on element k. Applying the divergence theorem

yields the following weak form

$$-\int_{\Omega_k} \varepsilon(\mathbf{r})\mathbf{E}_k(\mathbf{r})\cdot\nabla\ell_i(\mathbf{r})dV + \oint_{\partial\Omega_k} \hat{\mathbf{n}}(\mathbf{r})\cdot[\varepsilon(\mathbf{r})\mathbf{E}_k(\mathbf{r})]^*\ell_i(\mathbf{r})dS = \int_{\Omega_k}\rho(\mathbf{r})\ell_i(\mathbf{r})dV \quad (9)$$

$$\int_{\Omega_k} E_k^v(\mathbf{r})\ell_i(\mathbf{r})dV - \int_{\Omega_k}\varphi_k(\mathbf{r})\frac{\partial}{\partial v}\ell_i(\mathbf{r})dV + \oint_{\partial\Omega_k}\hat{n}_v(\mathbf{r})\varphi_k(\mathbf{r})^*\ell_i(\mathbf{r})dS = 0. \quad (10)$$

Here $\ell_i(\mathbf{r})$, $i = 1,\ldots,N_p$, are p-th order interpolating Lagrange polynomials [21], $N_p = (p+1)(p+2)(p+3)/6$ denotes the number of interpolating nodes, and $v \in \{x,y,z\}$ denotes the components of $\mathbf{E}(\mathbf{r})$ in the Cartesian coordinate system. We note here $\varphi_k(\mathbf{r})$ and $\mathbf{E}_k(\mathbf{r})$ denote the local solutions on element k and the global solutions on Ω are the direct sum of the local solutions.

φ^* and $(\varepsilon\mathbf{E})^*$ are numerical fluxes "connecting" element k to its neighboring elements. Here, the variables are defined on the interface between elements and the dependency on $\mathbf{r}$ is dropped for simplicity of notation. In LDG, the alternate flux [18]

$$\varphi^* = \{\varphi\} + 0.5\hat{\boldsymbol{\beta}}\cdot\hat{\mathbf{n}}\,[\![\varphi]\!]$$
$$(\varepsilon\mathbf{E})^* = \{\varepsilon\mathbf{E}\} - 0.5\hat{\boldsymbol{\beta}}(\hat{\mathbf{n}}\cdot[\![\varepsilon\mathbf{E}]\!]) - \tau\,[\![\varphi]\!]$$

is used in the interior of Ω, where the "average" and "jump" operators are defined as $\{\odot\} = 0.5(\odot^+ + \odot^-)$ and $[\![\odot]\!] = \odot^- - \odot^+$, respectively (here $\odot$ could be a scalar or a vector). Superscripts "$-$" and "$+$" refer to variables defined in element k and in its neighboring element, respectively. $-\tau\,[\![\varphi]\!]$ is a stabilization term introduced to penalize the non-physical oscillating eigenvectors corresponding to zero eigenvalues of the discretized system [21]. The vector $\boldsymbol{\beta}$ determines the upwind direction of φ and $(\varepsilon\mathbf{E})$. In LDG, it is essential to choose opposite directions for φ and $(\varepsilon\mathbf{E})$, while the precise direction of each variable is not important [18], [21], [22]. Here we choose $\hat{\boldsymbol{\beta}} = \hat{\mathbf{n}}$ on each element surface, which means that we always use $\varphi^* = \varphi^-$ and $(\varepsilon\mathbf{E})^* = (\varepsilon\mathbf{E})^+$. On boundaries, the numerical fluxes are chosen as $\varphi^* = f^D$ and $(\varepsilon\mathbf{E})^* = (\varepsilon\mathbf{E})^-$ on $\partial\Omega^D$ and $\varphi^* = \varphi^-$ and $(\varepsilon\mathbf{E})^* = f^N$ on $\partial\Omega^N$.

We expand $\varphi_k(\mathbf{r})$ and $E_{v,k}(\mathbf{r})$ with the same set of Lagrange polynomials $\ell_i(\mathbf{r})$ [21]

$$\varphi_k(\mathbf{r}) \simeq \sum_{i=1}^{N_p}\varphi(\mathbf{r}_i)\ell_i(\mathbf{r}) = \sum_{i=1}^{N_p}\varphi_k^i\ell_i(\mathbf{r}) \quad (11)$$

$$E_k^v(\mathbf{r}) \simeq \sum_{i=1}^{N_p}E_v(\mathbf{r}_i)\ell_i(\mathbf{r}) = \sum_{i=1}^{N_p}E_k^{v,i}\ell_i(\mathbf{r}) \quad (12)$$

where $\mathbf{r}_i$ denote the location of interpolating nodes, φ_k^i and $E_k^{v,i}$, $v \in \{x,y,z\}$, $k = 1,\ldots,K$, are the unknown coefficients to be solved for. Substituting (12) into (9) and (10), the weak form is converted into a global matrix system

$$\begin{bmatrix}\bar{T} & \bar{D}\bar{\varepsilon}\\ \bar{G} & \bar{M}\end{bmatrix}\begin{bmatrix}\bar{\Phi}\\ \bar{E}\end{bmatrix} = \begin{bmatrix}\bar{B}^{\varphi}\\ \bar{B}^{\mathbf{E}}\end{bmatrix}. \quad (13)$$

Here, the global unknown vectors $\bar{\Phi} = [\bar{\Phi}_1,\ldots,\bar{\Phi}_K]^T$ and $\bar{E} = [\bar{E}_1^x,\bar{E}_1^y,\bar{E}_1^z,\ldots,\bar{E}_K^x,\bar{E}_K^y,\bar{E}_K^z]^T$ are assembled from element-wise vectors $\bar{\Phi}_k = [\varphi_k^1,\ldots,\varphi_k^{N_p}]$ and $\bar{E}_k^v = [E_k^{v,1},\ldots,E_k^{v,N_p}]$, $v \in \{x,y,z\}$. The dimension of (13) can be further reduced by using the Schur complement, $\bar{E} = \bar{M}^{-1}(\bar{B}^{\mathbf{E}} - \bar{G}\bar{\Phi})$, which results in

$$(\bar{T} - \bar{D}\bar{\varepsilon}\bar{M}^{-1}\bar{G})\bar{\Phi} = \bar{B}^{\varphi} - \bar{D}\bar{\varepsilon}\bar{M}^{-1}\bar{B}^{\mathbf{E}}. \quad (14)$$

In (13) and (14), $\bar{M}$ is the mass matrix, which is a $K\times K$ block diagonal matrix, with each diagonal block being a 3×3 block diagonal matrix with 3 identical $N_p\times N_p$ blocks defined as

$$\bar{M}_{kk}^{(m)}(i,j) = \int_{\Omega_k}\ell_i(\mathbf{r})\ell_j(\mathbf{r})dV, \quad m = 1,2,3.$$

$\bar{\varepsilon}$ is a diagonal matrix with entries $(\bar{\varepsilon}_1,\ldots,\bar{\varepsilon}_K)$, where $\bar{\varepsilon}_k = (\bar{\varepsilon}_k^x,\bar{\varepsilon}_k^y,\bar{\varepsilon}_k^z)$, $\bar{\varepsilon}_k^v(i) = \varepsilon_k(\mathbf{r}_i)$, $k = 1,\ldots,K$, $v \in \{x,y,z\}$. We note that $\varepsilon(\mathbf{r})$ is assumed isotropic and constant in each element.

Matrices $\bar{G}$ and $\bar{D}$ represent the gradient and divergence operators, respectively. For LDG, one can show that $\bar{D} = -\bar{G}^T$ [19]. The gradient matrix $\bar{G}$ is a $K\times K$ block sparse matrix, where each block is of size $3N_p\times N_p$ and has contribution from the second volume integral term and the surface integral term in (10). The volume integral term only contributes to diagonal blocks as $\bar{G}_{kk}^{\text{vol}} = \left[\bar{S}_k^x\ \bar{S}_k^y\ \bar{S}_k^z\right]^T$, where

$$\bar{S}_k^v(i,j) = -\int_{\Omega_k}\ell_i(\mathbf{r})\frac{d\ell_j(\mathbf{r})}{dv}dV, \quad v \in \{x,y,z\}.$$

The surface integral term contributes to both the diagonal blocks $\bar{G}_{kk}$ and off-diagonal blocks $\bar{G}_{kk'}$, where k' corresponds to elements connected to element k, $k' \neq k$. Let $\partial\Omega_{kk'}$ be the interface connecting elements k and k', and let $\theta_k(j)$ selects the interface nodes from element k,

$$\theta_k(j) = \begin{cases}1, & \mathbf{r}_j \in \Omega_k,\ \mathbf{r}_j \in \partial\Omega_{kk'}\\ 0, & \text{otherwise.}\end{cases}$$

Then, the contribution of the surface integral term to the diagonal block and the off-diagonal blocks are $\bar{G}_{kk}^{\text{surf}} = \left[\bar{L}_k^x\ \bar{L}_k^y\ \bar{L}_k^z\right]^T$ and $\bar{G}_{kk'}^{\text{surf}} = \left[\bar{L}_{k'}^x\ \bar{L}_{k'}^y\ \bar{L}_{k'}^z\right]^T$, where

$$\bar{L}_k^v(i,j) = \frac{1+sign(\hat{\boldsymbol{\beta}}\cdot\hat{\mathbf{n}})}{2}\theta_k(j)\oint_{\partial\Omega_{kk'}}\hat{n}_v(\mathbf{r})\ell_i(\mathbf{r})\ell_j(\mathbf{r})dS,$$

and

$$\bar{L}_{k'}^v(i,j) = \frac{1-sign(\hat{\boldsymbol{\beta}}\cdot\hat{\mathbf{n}})}{2}\theta_{k'}(j)\oint_{\partial\Omega_{kk'}}\hat{n}_v(\mathbf{r})\ell_i(\mathbf{r})\ell_j(\mathbf{r})dS$$

respectively, $v \in \{x,y,z\}$. Special care needs to be taken on the domain boundaries where element k' does not exist. On $\partial\Omega^D$, the numerical flux is chosen as $\varphi^* = f_D$ and

$(\varepsilon\mathbf{E})^* = (\varepsilon\mathbf{E})^-$, which means $\hat{\boldsymbol{\beta}} = -\hat{\mathbf{n}}$ and only the off-diagonal term $\bar{G}^{\text{surf}}_{kk'}$ has nonzero contribution to the numerical flux. Because $\varphi^* = f^D$ is a known value, the contribution is moved to the right hand side. Similarly, on $\partial\Omega^N$, $\varphi^* = \varphi^-$ and $(\varepsilon\mathbf{E})^* = f^N$, meaning that $\hat{\boldsymbol{\beta}} = \hat{\mathbf{n}}$ and only $\bar{G}^{\text{surf}}_{kk}$ has nonzero contribution.

Matrix $\bar{T}$ is the stabilization operator corresponds to the stabilization term in the numerical flux. It is a $K \times K$ block sparse matrix $N_p \times N_p$ blocks. The diagonal and off-diagonal blocks are

$$\bar{T}_{kk}(i,j) = -\tau\theta_k(j)\oint_{\partial\Omega_{kk'}} \ell_i(\mathbf{r})\ell_j(\mathbf{r})dS$$

and

$$\bar{T}_{kk'}(i,j) = \tau\theta_{k'}(j)\oint_{\partial\Omega_{kk'}} \ell_i(\mathbf{r})\ell_j(\mathbf{r})dS.$$

Finally, the right hand side terms correspond to the force term and boundary conditions as

$$\bar{B}^{\varphi}_k(i) = \int_{\Omega_k} f(\mathbf{r})\ell_i(\mathbf{r})dV + \oint_{\partial\Omega_k\cap\partial\Omega^N} f^N(\mathbf{r})\ell_i(\mathbf{r})dS \quad (15)$$

$$\bar{B}^{\mathbf{E},\nu}_k(i) = \oint_{\partial\Omega_k\cap\partial\Omega^D} \hat{n}_\nu(\mathbf{r})f^D(\mathbf{r})\ell_i(\mathbf{r})dS, \quad \nu \in \{x,y,z\}. \quad (16)$$

C. FLOATING POTENTIAL BOUNDARY CONDITION

Having described the LDG method in the previous section, we now introduce the FPBC (4) on the boundary of an FPC. Consider conductor η, the first condition in (4) requires all potential values on $\partial\Omega^C_\eta$ to be equal to a single value φ^C_η. This is similar to the Dirichlet boundary condition. Hence, we enforce the boundary condition through the numerical flux as $\varphi^* = \varphi^C_\eta$ and $(\varepsilon\mathbf{E})^* = (\varepsilon\mathbf{E})^-$. On $\partial\Omega^C_\eta$, the surface integral term in (10) becomes

$$\oint_{\partial\Omega_k} \hat{n}_\nu(\mathbf{r})\varphi^C_\eta\ell_i(\mathbf{r})dS, \quad i = 1,2,\ldots,N_p, \ \mathbf{r} \in \partial\Omega^C_\eta$$

However, different from the Dirichlet boundary condition, φ^C_η is an unknown and therefore we can not simply move the above integral to the right hand side as done in (16). Therefore we add φ^C_η as an unknown to the linear system (13). But then, an additional equation is needed. This equation is precisely the charge condition in (4). This condition can be expressed as

$$\oint_{\partial\Omega^C_\eta} \hat{\mathbf{n}}(\mathbf{r})\cdot\varepsilon(\mathbf{r})\mathbf{E}(\mathbf{r})d\mathbf{r} = Q^C_\eta, \quad \mathbf{r} \in \partial\Omega^C_\eta.$$

The above conditions are implemented in two steps. First, add one column $\bar{G}^C_\eta$ to $\bar{G}$ to set the numerical flux φ^* on $\partial\Omega^C_\eta$ to be a single value φ^C_η,

$$\bar{G}^C_\eta = \left[\bar{G}^{C,x}_{\eta,1}, \bar{G}^{C,y}_{\eta,1}, \bar{G}^{C,z}_{\eta,1}, \ldots, \bar{G}^{C,x}_{\eta,K}, \bar{G}^{C,y}_{\eta,K}, \bar{G}^{C,z}_{\eta,K}\right]^T$$

where

$$\bar{G}^{C,\nu}_{\eta,k}(i) = \oint_{\partial\Omega_k\cap\partial\Omega^C_\eta} \hat{n}_\nu(\mathbf{r})\ell_i(\mathbf{r})dS, \quad \nu \in \{x,y,z\}.$$

Second, add one row $\bar{F}^C_\eta$ to $\bar{D}\bar{\varepsilon}$ to enforce the total electric flux on $\partial\Omega^C_\eta$ to be a single value Q^C_η:

$$\bar{F}^C_\eta = \left[\bar{F}^{C,x}_{\eta,1}, \bar{F}^{C,y}_{\eta,1}, \bar{F}^{C,z}_{\eta,1}, \ldots, \bar{F}^{C,x}_{\eta,K}, \bar{F}^{C,y}_{\eta,K}, \bar{F}^{C,z}_{\eta,K}\right]$$

where

$$\bar{F}^{C,\nu}_{\eta,k}(i) = \oint_{\partial\Omega_k\cap\partial\Omega^C_\eta} \hat{n}_\nu(\mathbf{r})\varepsilon(\mathbf{r})\ell_i(\mathbf{r})dS, \quad \nu \in \{x,y,z\}.$$

Then, the matrix system becomes

$$\begin{bmatrix} \tilde{T} & \tilde{D} \\ \tilde{G} & \tilde{M} \end{bmatrix}\begin{bmatrix} \tilde{\Phi} \\ \tilde{E} \end{bmatrix} = \begin{bmatrix} \tilde{B}^{\varphi} \\ \tilde{B}^{\mathbf{E}} \end{bmatrix} \quad (17)$$

where

$$\tilde{T} = \begin{bmatrix} \bar{T} & 0 \\ 0 & 0 \end{bmatrix}, \quad \tilde{G} = [\bar{G}, \bar{G}^C_\eta], \ \tilde{D} = \begin{bmatrix} \bar{D}\bar{\varepsilon} \\ \bar{F}^C_\eta \end{bmatrix},$$
$$\tilde{\Phi} = \begin{bmatrix} \bar{\Phi} \\ \varphi^C_\eta \end{bmatrix}, \quad \tilde{B}^{\varphi} = \begin{bmatrix} \bar{B}^{\varphi} \\ Q^C_\eta \end{bmatrix}.$$

Eliminating $\tilde{E}$ using Schur complement, one can obtain the reduced linear system

$$(\tilde{T} - \tilde{D}\bar{M}^{-1}\tilde{G})\tilde{\Phi} = \tilde{B}^{\varphi} - \tilde{D}\bar{M}^{-1}\bar{B}^{\mathbf{E}}. \quad (18)$$

This procedure can be generalized to an arbitrary number of isolated FPCs by simply adding multiple variables φ^C_η, $\eta = 1,2,\ldots M$, and correspondingly, M rows and columns as described above.

In practice, one can avoid changing the matrix size. Note that all unknowns φ^i_k on one FPBC are equal to a single value φ^C_η, we can simply choose a reference node on that FPC boundary and set the numerical flux φ^* associated with all φ^i_k on the same boundary as the unknown of the reference node. Assume that the row index of the reference node is m in $\bar{\Phi}$, then the two modification steps to (13) become:

- Step (I): Add $\bar{G}^C_\eta$ to the m-th column of $\bar{G}$
- Step (II): Add $\bar{F}^C_\eta$ to the m-th row of $\bar{D}\bar{\varepsilon}$ and add Q^C_η to the m-th row of $\bar{B}^{\varphi}$

Here, one has the freedom of choosing any node on a given FPC boundary as the reference node in Step (I), while the charge condition added in Step (II) ensures that the solution is unique. For cases with multiple FPCs, an individual reference node is defined for each FPC. With the modified submatrices, the reduced linear system has the same form as (14).

III. NUMERICAL EXAMPLES

A. COAXIAL CAPACITOR WITH FPC

To validate the proposed method, first, we consider a two dimensional canonical problem that involves an isolated thin metallic tube inserted into a coaxial capacitor. The schematic describing the problem is provided in Figure 2a. The isolated tube is modeled as an FPC surface. The radii of the inner metallic core, the outer metallic boundary, the inner surface of the FPC, and the outer surface of the FPC are r_0, r_1, r_2, and r_3, respectively. The total charge on the FPC is Q. It assumed that the potential on the surface of the core and the outer

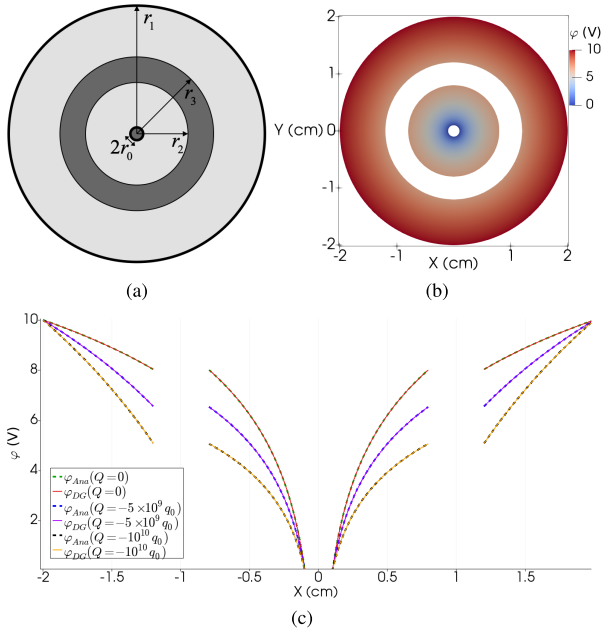

FIGURE 2. **(a) Schematic description of the coaxial capacitor model. (b) φ solved from the proposed DG method. (c) Comparison of analytic and numerical solutions of φ on the line $(x, y = 0)$.**

boundary are known, $\varphi(r = r_0) = V_0$ and $\varphi(r = r_1) = V_1$. Then the potential everywhere inside the outer boundary has an analytical expression

$$\varphi(r,\theta) = \begin{cases} a_0 + b_0 \ln(r), & r \in [r_0, r_2] \\ a_1 + b_1 \ln(r), & r \in [r_3, r_1]. \end{cases}$$

Here, $a_0 = V_0 - b_0 \ln(r_0)$, $a_1 = V_1 - b_e \ln(r_1)$, $b_0 = b_1 + Q/(2\pi\varepsilon)$, $b_1 = [V_0 - V_0 - C_{20}Q/(2\pi\varepsilon)]/(C_{20} - C_{31})$, and $C_{ij} = \ln(r_i/r_j)$. For the numerical experiments described below, $V_0 = 0$, $V_1 = 10$ V, $r_0 = 0.1$ cm, $r_1 = 2$ cm, $r_2 = 0.8$ cm and $r_3 = 1.2$ cm.

We first assume that the FPC is electrically neutral, i.e., $Q = 0$. The DG method uses first-order basis functions for a fair comparison with VPM and MRM, which are first-order methods. Figure 2b shows the electric potential computed using the DG method. Figure 2c compares the DG solution with the analytical solution along the line $(x, y = 0)$. One can see the numerical solution agrees very well with the analytical solution.

Using the analytical expression above, one can find that the value of the potential on the FBC is $\varphi_f^{\text{Ana}} = 8.027904$ V. This value is also computed using DG, MRM, and VMP with different values of virtual permittivity ϵ_v (all methods use the same mesh but for DG mesh elements internal to the FPC are removed). Table. 2 summarizes the results. Second column is the floating potential value φ_f as computed by the numerical schemes, third column is the difference with respect to the analytical solution: $\text{diff}_f = |\varphi_f - \varphi_f^{\text{Ana}}|$, and fourth column is the condition number of the matrix. We should note here that VMP does not produce a single value for the floating potential (especially for low values of ϵ_v), therefore φ_f for VMP is selected as the value that produces the maximum diff_f. The table shows that, for DG and MRM, the errors are on the same level while the accuracy of VPM depends on the choice of ϵ_v (as reported in [15]). For smaller values of ϵ_v, the virtual material does not behave like a perfect conductor. For larger values of ϵ_v, the FEM matrix becomes more and more ill-conditioned, which eventually results in an inaccurate solution.

TABLE 2. **Comparison of different methods in the coaxial capacitor example.**

Method	φ_f (V)	diff_f (V)	Condition number
DG-FPBC	8.027886	1.828×10^{-5}	1.329×10^{8}
MRM	8.027876	2.833×10^{-5}	2.267×10^{6}
VPM, $\epsilon_v = 10^4$	8.026895	1.009×10^{-3}	1.228×10^{8}
VPM, $\epsilon_v = 10^6$	8.027030	8.744×10^{-4}	1.228×10^{10}
VPM, $\epsilon_v = 10^8$	8.027031	8.730×10^{-4}	1.228×10^{12}
VPM, $\epsilon_v = 10^{10}$	8.026730	1.174×10^{-3}	1.228×10^{14}
VPM, $\epsilon_v = 10^{12}$	7.907102	1.208×10^{-1}	1.223×10^{16}

For the second case, we assume that there are charges residing on the FPC, i.e., $Q \neq 0$. In this case, the accuracy of the DG method is verified against only the analytical solution since VPM and MRM cannot directly account for charges located on an FPC [15]. Figure 2c plots the electric potential computed by the DG method and using the analytical expression above along the line $(x, y = 0)$ for two cases with $Q = -5 \times 10^9\, q_0$ and $Q = -10^{10} q_0$, where q_0 is the electron charge. The figure shows that the DG solutions match with the analytical results very well. The errors are at the same level as in the $Q = 0$ case: For $Q = -5 \times 10^9\, q_0$, $\text{diff}_f = 7.787 \times 10^{-6}$ V and for $Q = -10^{10} q_0$, $\text{diff}_f = 1.311 \times 10^{-5}$ V.

B. PLASMONIC-ENHANCED PHOTOCONDUCTIVE ANTENNA

Next, we consider a practical three dimensional example. In recent years, nanostructures have become common components of optoelectronic devices since they significantly enhance the interaction between optical electromagnetic waves and semiconductor material often resulting in increased device performance [23]. Modeling these devices calls for solving two sets of equations: (i) a steady-state system modeling interactions of DC electric field and carrier densities and (ii) a transient-state system modeling interactions of high-frequency electromagnetic waves and carrier densities. The solution of steady-state system provides not only the initial state for the transient system but also the DC electric field that persists throughout the transient response. Moreover, the field-dependent mobility obtained from the steady-state solution is needed in the transient simulation. Hence, an accurate solution of the steady-state system is essential for correctly modeling these devices.

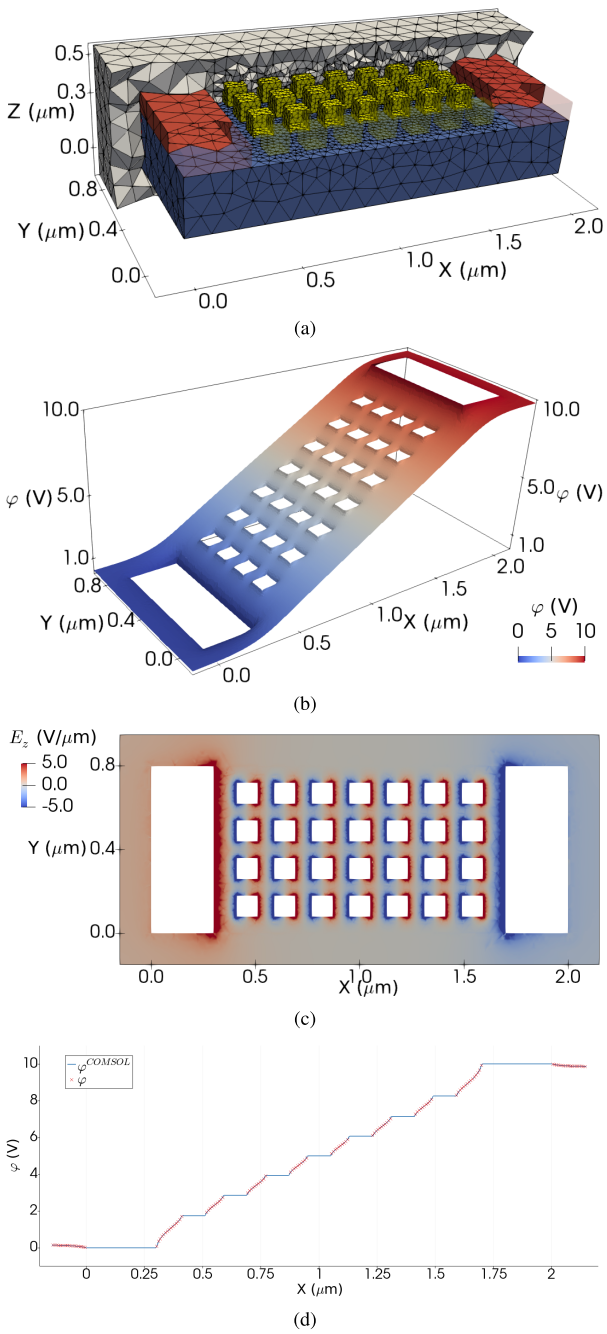

FIGURE 3. (a) Structure of the plasmonic-enhanced PCA and corresponding mesh used in the proposed DG method. (b) φ and (c) E_z on the plane $(x, y, z = 0.3\mu m)$ solved from the proposed DG method. (d) φ on the line $(x, y = 0.3\mu m, z = 0.3\mu m)$ solved from the proposed DG method and COMSOL multiphysics.

The semiclassical approach for semiconductor devices models the steady-state in the form of a coupled system of Poisson equation (describing the behavior of the electric potential) and drift-diffusion/hydrodynamic equations (describing the behavior of the carrier densities). In many of the optoelectronic device designs, the nanostructures are isolated conductors that not directly connected to any electrode [7]. This calls for solution of the Poisson equation with an FPC.

Here, we consider the device component of a plasmonic-enhanced photoconductive antenna (PCA) and solve the pertinent electrostatic problem. Figure 3 shows a typical configuration [7] of the device. Dirichlet boundary condition is enforced on the surface of the electrodes (shown in red in the figure). The left electrode is the cathode with $\varphi(\mathbf{r}) = 0$ and the right electrode is the anode with $\varphi(\mathbf{r}) = 10$ V. The nanostructures (shown in yellow in the figure) are the FPCs and each block is modeled by enforcing an independent FPBC on its surface. The semiconductor layer (shown in blue in the figure) has relative dielectric permittivity of 10.9 and the surrounding area (shown in gray in the figure) is vacuum. The computation domain is truncated at the outmost boundaries with the homogeneous Neumann boundary condition.

Figure 3b shows the electric potential computed by the DG method on the plane $(x, y, z = 0.3\mu m)$. The figure clearly shows that $\varphi(\mathbf{r})$ is constant on the surface of each FPC block. The potential values on different FPC blocks change along the x direction significantly while staying approximately the same along the y direction. These results presented in this figure demonstrate that the nanostructures not only interact with optical electromagnetic waves (which is the original reason for introducing them into the optoelectronic device), but also change the local (static) electric potential. In fact, the static electric field $\mathbf{E}(\mathbf{r}) = -\nabla\varphi(\mathbf{r})$ becomes very strong in vicinity of the nanostructures. For example, see the E_z component shown in Figure 3c. This can greatly influence the carrier mobilities in the semiconductor layer [24] and therefore change the device performance.

The electric potential computed using the DG method is verified against that computed using the commercial software package COMSOL multiphysics. Figure 3a plots the solutions on the line $(x, y = 0.3\mu m, z = 0.3\mu m)$. The maximum difference between the solutions, $\max(|\varphi(\mathbf{r}) - \varphi^{\mathrm{COMSOL}}(\mathbf{r})|)$, is $0.0314V$. Note that while computing the difference, we have interpolated $\varphi^{\mathrm{COMSOL}}$ to the nodal points of the DG method.

We should also mention here that, since the FPCs are treated as boundary conditions, volumetric meshes are not required inside the FPCs. This is shown in Figure 3, where some mesh elements are made transparent intentionally for visualization purposes. This treatment saves significant amount of computational resources since the nanostructures usually require finer meshes.

IV. CONCLUSION

In this work, we report a new approach to model FPCs within a DG-based numerical framework. This approach permits both the equipotential condition and the charge condition (collectively termed as FPBC) to be enforced on the surface of an FPC. As a result, nonzero charge conditions are easily and "naturally" taken into account. We should note here that directly enforcing such nonzero charge conditions in FEM is not a trivial task and to the best of our knowledge it has not been reported in the literature yet. Unlike the popular VPM, the FPBC does not degrade the accuracy of the original

DG solver. At the same time, the implementation of FPBC only requires simple changes to the original code.

The main disadvantage of DG over FEM is the larger number of unknowns due to the nodal duplication at element interfaces. Nevertheless, by treating FPC as (surface) boundary conditions and therefore removing the volumetric meshes internal to them, the number of unknowns can be reduced. A further reduction can be achieved by using coarser meshes with higher order basis functions [21]. Note that defining higher order basis functions is easier within DG than FEM. Our future work includes development of extensions of the DG method to account for non-conformal meshes and to make use of local h-/p- refinement strategies. These extensions will significantly increase efficiency of the simulation especially for complex geometries.

REFERENCES

[1] J. C. Aracil, J. Lopez-Roldan, J. C. Coetzee, T. Tang, and F. Darmann, "Electrical insulation of high voltage inductor with co-axial electrode at floating voltage," *IEEE Trans. Dielectr. Electr. Insul.*, vol. 21, no. 3, pp. 1053–1060, Jun. 2014.

[2] Z. Andjelic, K. Ishibashi, and P. Di Barba, "Novel double-layer boundary element method for electrostatic analysis," *IEEE Trans. Dielectr. Electr. Insul.*, vol. 25, no. 6, pp. 2198–2205, Dec. 2018.

[3] F. Zeng, J. Tang, X. Zhang, S. Zhou, and C. Pan, "Typical internal defects of gas-insulated switchgear and partial discharge characteristics," in *Proc. Simulation Modelling Elect. Insul. Weaknesses Elect. Equip.*, 2018, p. 103.

[4] H. Zildzo, A. Muharemovic, I. Turkovic, and H. Matoruga, "Numerical calculation of floating potentials for large earthing system," in *Proc. 22nd Int. Symp. Inf., Commun. Autom. Technol.*, Oct. 2009, pp. 1–6.

[5] D. Kahng and S. M. Sze, "A floating gate and its application to memory devices," *Bell Syst. Tech. J.*, vol. 46, no. 6, pp. 1288–1295, Jul. 1967.

[6] L. Goembel, "Plasma analyzer for measuring spacecraft floating potential in LEO and GEO," *IEEE Trans. Plasma Sci.*, vol. 40, no. 2, pp. 155–166, Feb. 2012.

[7] S.-G. Park, Y. Choi, Y.-J. Oh, and K.-H. Jeong, "Terahertz photoconductive antenna with metal nanoislands," *Opt. Express*, vol. 20, no. 23, pp. 25530–25535, Nov. 2012.

[8] F. Roman, V. Cooray, and V. Scuka, "Comparison of the breakdown of rod-plane gaps with floating electrode," *IEEE Trans. Dielectr. Electr. Insul.*, vol. 5, no. 4, pp. 622–624, Aug. 1998.

[9] D. Amann, A. Blaszczyk, G. Of, and O. Steinbach, "Simulation of floating potentials in industrial applications by boundary element methods," *J. Math. Ind.*, vol. 4, no. 1, p. 13, Oct. 2014.

[10] A. Konrad and M. Graovac, "The finite element modeling of conductors and floating potentials," *IEEE Trans. Magn.*, vol. 32, no. 5, pp. 4329–4331, Sep. 1996.

[11] A. Blaszczyk and H. Steinbigler, "Region-oriented charge simulation," *IEEE Trans. Magn.*, vol. 30, no. 5, pp. 2924–2927, Sep. 1994.

[12] T. Takuma and T. Kawamoto, "Numerical calculation of electric fields with a floating conductor," *IEEE Trans. Dielectr. Electr. Insul.*, vol. 4, no. 2, pp. 177–181, Apr. 1997.

[13] W. Dong, R. Jiangjun, D. Zhiye, L. Shoubao, and Z. Yujiao, "Parallel numerical computing of finite element model of conductors and floating potentials," in *Proc. Int. Symp. Parallel Distrib. Process. Appl.*, Sep. 2010, pp. 57–61.

[14] W. N. Fu, S. L. Ho, S. Niu, and J. Zhu, "Comparison study of finite element methods to deal with floating conductors in electric field," *IEEE Trans. Magn.*, vol. 48, no. 2, pp. 351–354, Feb. 2012.

[15] D. Rincon, E. Aguilera, and J. Chacón, "Numerical treatment of floating conductors based on the traditional finite element formulation," *Adv. Electromagn.*, vol. 7, no. 3, pp. 46–55, Aug. 2018.

[16] X. Dong, F. Qu, Y. Li, Z. Wu, Z. Chen, G. Huang, and G. Liu, "Calculation of 3-D electric field intensity in presence of conductors with floating potentials," in *Proc. IEEE 12th Int. Conf. Properties Appl. Dielectr. Mater. (ICPADM)*, May 2018, pp. 351–354.

[17] G. Aiello, S. Alfonzetti, S. A. Rizzo, and N. Salerno, "FEM-DBCI solution of open-boundary electrostatic problems in the presence of floating potential conductors," *IEEE Trans. Magn.*, vol. 52, no. 3, pp. 1–4, Mar. 2016.

[18] B. Cockburn and C.-W. Shu, "The local discontinuous Galerkin method for time-dependent convection-diffusion systems," *SIAM J. Numer. Anal.*, vol. 35, no. 6, pp. 2440–2463, Dec. 1998.

[19] P. Castillo, B. Cockburn, I. Perugia, and D. Schötzau, "An a priori error analysis of the local discontinuous Galerkin method for elliptic problems," *SIAM J. Numer. Anal.*, vol. 38, no. 5, pp. 1676–1706, Jan. 2000.

[20] L. Chen and H. Bagci, "A discontinuous Galerkin framework for multiphysics simulation of photoconductive devices," in *Proc. Int. Appl. Comput. Electromagn. Soc. Symp. (ACES)*, Apr. 2019, pp. 1–2.

[21] J. S. Hesthaven and T. Warburton, *Nodal Discontinuous Galerkin Methods: Algorithms, Analysis, and Applications*. New York, NY, USA: Springer, 2008.

[22] C.-W. Shu, "Discontinuous Galerkin methods for time-dependent convection dominated problems: Basics, recent developments and comparison with other methods," in *Building Bridges: Connections and Challenges in Modern Approaches to Numerical Partial Differential Equations*. Cham, Switzerland: Springer, 2016, pp. 371–399.

[23] J. Piprek, Ed., *Handbook of Optoelectronic Device Modeling and Simulation*. Boca Raton, FL, USA: CRC Press, 2018.

[24] K. Moon, I.-M. Lee, J.-H. Shin, E. S. Lee, W.-H. Lee, H. Ko, S. Han, and K. H. Park, "Bias field tailored plasmonic nano-electrode for high-power terahertz photonic devices," *Sci. Rep.*, vol. 5, Sep. 2012, Art. no. 13817.

LIANG CHEN (Member, IEEE) received the B.S. degree in applied physics from Southeast University, Nanjing, China, in 2007, and the M.S. and Ph.D. degrees in microelectronic and solid-state electronics from the Shanghai Institute of Microsystem and Information Technology, Chinese Academy of Sciences, Shanghai, China, in 2009 and 2012, respectively. From 2012 to 2013, he was a High-Performance Computing Engineer with the HPC Solution Center, Dawning Information Industry Company Ltd. From 2013 to 2017, he was the Principal Developer of the Electromagnetics Simulation Software EastWave. He has served as the Director of the Technical Solution Department, DongJun Technology Company Ltd. Since 2017, he joined the King Abdullah University of Science and Technology (KAUST), Thuwal, Saudi Arabia, as a Postdoctoral Research Fellow. His research interests include computational physics (electromagnetics, semiconductor devices, quantum transport, and multiphysics simulation), computer-aided engineering software, high-performance computing, and various topics in photonics and condensed matter physics.

MING DONG (Student Member, IEEE) received the bachelor's degree in electronic information science and technology from Lanzhou University, Lanzhou, China, and the master's degree in electrical engineering from the King Abdullah University of Science and Technology, Saudi Arabia, in 2018, where he is currently pursuing the Ph.D. degree.

His current research interests include the time-domain finite-element method, time-domain discontinuous Galerkin method and its application in electromagnetic scattering analysis, semiconductor devices simulation, and multiphysics simulation.

HAKAN BAGCI (Senior Member, IEEE) received the B.S. degree in electrical and electronics engineering from Bilkent University, Ankara, Turkey, in 2001, and the M.S. and Ph.D. degrees in electrical and computer engineering from the University of Illinois at Urbana–Champaign (UIUC), Urbana, IL, USA, in 2003 and 2007, respectively.

From June 1999 to July 2001, he worked as an Undergraduate Researcher with the Computational Electromagnetics Group, Bilkent University. From August 2001 to December 2006, he was a Research Assistant with the Center for Computational Electromagnetics and the Electromagnetics Laboratory, UIUC. From January 2007 to August 2009, he was a Research Fellow with the Radiation Laboratory, University of Michigan, Ann Arbor, MI, USA. Since August 2009, he has been with the King Abdullah University of Science and Technology (KAUST), Thuwal, Saudi Arabia, where he is currently an Associate Professor of electrical engineering. He has authored or coauthored more than 90 journal articles and more than 200 papers in conference proceedings. His research interests include various aspects of theoretical and applied computational electromagnetics with emphasis on well-conditioned frequency and time domain integral equation formulations and their discretization, hybrid time domain integral and differential equation solvers, accurate, stable, and efficient marching schemes for time domain solvers, stochastic characterization of electromagnetic field, and wave interactions on complex geometries, and solution of two and three dimensional electromagnetic inverse scattering problem using signal processing techniques. He was a recipient of the 2008 International Union of Radio Scientists (URSI) Young Scientist Award and the 2004–2005 Interdisciplinary Graduate Fellowship from the Computational Science and Engineering Department, UIUC. His article titled Fast and Rigorous Analysis of EMC/EMI Phenomena on Electrically Large and Complex Structures Loaded With Coaxial Cables was one of the three finalists (with honorable mention) for the 2008 Richard B. Schulz Best Transactions Paper Award given by the IEEE Electromagnetic Compatibility Society. He has authored (as student) or coauthored (as student and advisor) 17 finalist/honorable mention articles in the student paper competitions at the 2005, 2008, 2010, 2014, 2015, 2016, 2017, 2018 IEEE Antennas and Propagation Society International Symposiums and the 2013, 2014, 2016, 2017, and 2018 Applied Computational Electromagnetics Society Conferences. He is currently an Associate Editor of the IEEE TRANSACTIONS ON ANTENNAS AND PROPAGATION, the IEEE JOURNAL ON MULTISCALE AND MULTIPHYSICS COMPUTATIONAL TECHNIQUES, and the *IEEE Antennas and Propagation Magazine*.